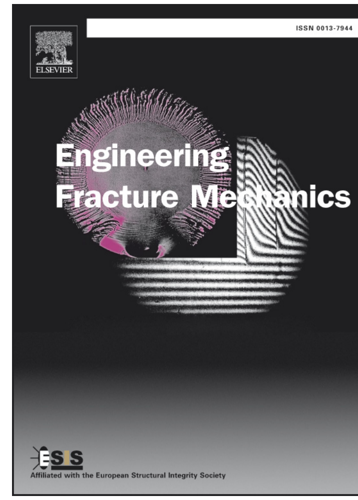

Damage based model to study the effect of notch introduction technique on the *J*-integral value of PolyOxyMethylene

Lucien Laiarinandrasana, Jonathan Ricard, Fabrice Guigné, Yin Cheng, Thilo F. Morgeneyer, Lukas Helfen

PII: S0013-7944(15)00482-8
DOI: http://dx.doi.org/10.1016/j.engfracmech.2015.08.031
Reference: EFM 4844

To appear in: *Engineering Fracture Mechanics*

Received Date: 5 November 2014
Revised Date: 20 July 2015
Accepted Date: 20 August 2015

Please cite this article as: Laiarinandrasana, L., Ricard, J., Guigné, F., Cheng, Y., Morgeneyer, T.F., Helfen, L., Damage based model to study the effect of notch introduction technique on the *J*-integral value of PolyOxyMethylene, *Engineering Fracture Mechanics* (2015), doi: http://dx.doi.org/10.1016/j.engfracmech.2015.08.031

Damage based model to study the effect of notch introduction technique on the J-integral value of PolyOxyMethylene

Lucien Laiarinandrasana[a,*], Jonathan Ricard[a], Fabrice Guigné[b], Yin Cheng[a,c], Thilo F. Morgeneyer[a], Lukas Helfen[c,d]

[a] *MINES ParisTech, PSL-Research University, MAT-Centre for Material Sciences, CNRS UMR7633, BP 87, 91003 Evry Cedex, France*
[b] *PSA Peugeot-Citroën, Route de Gisy, 78943 Vélizy-Villacoublay Cedex, France*
[c] *ANKA/Institute for Photon Science and Synchrotron Radiation, Karlsruhe Institute of Technology (KIT), D-76131 Karlsruhe, Germany*
[d] *European Synchrotron Radiation Facility (ESRF), BP 220, F-38043 Grenoble Cedex, France*

Abstract

Experimental data on a CT specimen made of PolyOxyMethylene were enriched by in-situ laminographic observations in 3D. The observed micro-mechanisms of crack initiation and growth have been simulated by using a damage based model. A critical value of J-integral was determined. The same model was utilized to simulate an initially heterogeneous porosity in the CT specimen to mimic the state of the material after a cutting process. A notch tip touching tool led to a less compliant specimen and a higher value of critical J_{cr} whereas non touching conditions, induced a damaged layer around the notch tip leading to a decrease in J_{cr}.

Keywords: Semi-crystalline polymers, Tomography, Laminography, Finite element, J-integral, Local approach to fracture

1. Introduction

The use of thermoplastic polymers in the automative industry has been increasing continuously in the last few decades, essentially due to their low density,

*Corresponding Author. E-mail adress: lucien.laiarinandrasana@mines-paristech.fr, Tel: +33 1 60 76 30 64, Fax: +33 1 60 76 31 50

ease of processing and also to environmental constraints. The assembling operation makes use of a screwing process. This study deals with screwing a metallic screw into a PolyOxyMethylene (POM) semi-crystalline polymer and is based essentially on results published in [18]. In this latter paper, the mechanisms of deformation, cavitation and failure of a POM were studied comprehensively by using various observation techniques including tomography. Modelling by using the local approach to fracture mechanics was utilized to simulate the screwing process. A failure assessment diagram was derived to evaluate the safety margin left after the assembling process with respect to the rotation speed of the screwer.

The present paper benefits from the damage based model elaborated in the previous study. The "damage" being defined here as the porosity or the void volume fraction f, which measurement is based on a concept of volume of interest (VOI) corresponding to (50 μm)^3 (containing about 50 to 100 spherulites) for the POM under study. f is then defined as the total volume of voids within the VOI, divided by the volume of this VOI.

The methods used to introduce a sharp crack into a fracture mechanics specimen (CT-like here) may change the state of the material near the crack tip. Indeed, this state may depend on that crack tip touching or non touching tool [16, 3, 20], involved in the sharp crack introducing technique. The present work aims at predicting the effects of such an initial state near the crack tip on the critical J-integral value.

Synchrotron radiation laminography (SR-CL) is a technique particularly adapted to the observation of regions of interest in flat specimens at micrometre resolution. SR-CL was then used to perform *in-situ* test on the CT-like specimen. The first part of the paper introduces the POM under study with its main physico-chemical characteristics. SR-CL results are then discussed in terms of macroscopic measurements (opening displacement and video acquisition at the surface of the sample), as well as microscopic description of the mechanisms of damage/cracking.

Section 3.1 details the finite element (FE) analysis based on a porous plastic constitutive model. It is shown that the mechanisms of crack intitiation and growth observed by SR-CT could be successfully simulated. Moreover the simulated load *versus* opening displacement curve could be produced. It was then possible to evaluate the J-integral by using the procedure proposed in [2] or in [7]. It should be mentioned that this study is within the framework of ESIS TC4 round robin [1], investigating the mechanisms of failure of polymers and in particular the uncertainties associated with the measurement of the crack advance Δa.

At last, crack tip touching and non touching conditions in the cutting process were supposed to set a variation of the initial porosity in a layer of elements ahead of the notch root. Carrying out simulations on various case studies gave a better understanding of the effects of the notch root state on the critical J-integral values at three specific events on the crack surface shape evolution.

2. Experiments

2.1. Material and CT-like specimen

The material under study was a semi-crystalline thermoplastic polyoxymethylene (POM) used in the automative industry and provided by ARaymond company [17, 18]. It is a semi-crystalline polymer, with a degree of crystallinity of about 40 %, measured by Differential Scanning Calorimetry (DSC). The glass transition temperature was estimated at -60 ° C by using the Dynamic Mechanical Thermal Analysis (DMTA) technique. Here, all the tests were carried out at room temperature (20°). The initial void volume fraction was assumed to be f_0=0.01.

Following the work in [18] and [14] the present paper is devoted to the study of the evolution of micro-cracks within a CT-like specimen using laminography technique. Fig. 1a shows a picture of a tested CT specimen, after crack growth at the end of the laminography experiment. The main dimensions of this specimen were: thickness $B = 2$ mm (instead of 1 mm in [18]), width $W = 40$mm, initial crack length $a_0 = 20$ mm. In order to set a reproducible crack tip and to fix the crack notch root radius, the notch was machined through the thickness, with an initial notch root radius of $\rho = 0.25$ mm. The effects of notch root radius on the stress-strain curves on the one hand and on the distribution of the void volume fraction within the net section on the other hand, were published elsewhere [17, 18]. From three studied notch root radii (ρ= 1 mm; 0.25 mm and 0.06mm), it was shown that the distributions of the porosity –hence the stress distribution in the vicinity of the crack tip – were similar when $\rho \leq 0.25$ mm.

2.2. Laminography setup

Synchrotron Radiation Computed Tomography (SR-CT) is particularly well adapted to imaging of one-dimensionally elongated objects (i.e., beam-like samples) that stay in the field of view of the detector system under rotation. In contrast, Synchrotron Radiation Computed Laminography (SR-CL) [9, 11, 10, 15] is optimised for the imaging of laterally extended (i.e., plate or sheet-like) specimens. For SR-CL, the rotation axis of the specimen is inclined at an angle less than 90° with respect to the beam direction (where 90 ° corresponds to the case of SR-CT). The specimens are typically turned around the normal vector of the sheet plane (see fig. 1b). For plate-like specimens this allows a relatively constant average X-ray transmission over the entire scanning range of 360°, which in turn allows for the acquisition of reliable projection.

Imaging was performed at the TopoTomo beamline of the ANKA synchrotron light source (Karlsruhe, Germany) [6]. An inclination angle of the specimen rotation axis of about 25° with respect to the beam normal (65°) was chosen. A white X-ray beam in a photon energy window of 9.6-24 keV with the maximum flux density located at 14.5 keV was used. Volumes were reconstructed from 2000 angularly equidistant radiographs; the exposure time of each projection was about 20 ms, guaranteeing a total scanning time of around 50 s for a single laminogram. The scanned region was 2.2 mm^3 in volume with a voxel size of 1.1 µm. The final reconstructed volumes have a size of 2016 x 2016 x 2016 voxels.

The loading has been applied by opening the notch mouth with a displacement controlled 2-screw opening device (fig. 1c), without measuring the load level. An anti-buckling device was been mounted around the specimen, leaving a window for the synchrotron X-ray laminography close to the notch to prevent the thin sheet from buckling in the compressive zone. The region of interest (ROI) for the scan was close to the notch. Between every scan 2D micrographs of the specimen notch region have been taken through this window with a CCD-camera. Stepwise loading has been applied between each laminography scan. The influence of the time dependent deformation was reduced by waiting more than 5 min before each laminography scan, allowing the short term stress relaxation to operate. This method has already been successfully applied for *in-situ* tensile test for polyamide 6 [14]. The applied total crack mouth opening displacements (δ) relevant to this work were respectively: δ = 0.5 mm and δ = 1.0 mm. The material is assumed to deform from the first loading step onwards.

2.2.1. Images at macroscopic scale

Fig. 2 illustrates three pictures taken before SR-CL inspections. The speckle pattern visible at the surface of the specimen allows a digital image correlation to be made and the crack tip opening displacement to be followed. The reference image in fig. 2a shows the notch root in a non deformed state. After an imposed δ of 0.5 mm (fig. 2b), the notch has been enlarged but no whitening was visible at the surface. When an opening displacement of δ= 1 mm was applied, a brittle crack appeared abruptly (fig. 2c). It can be observed that the crack direction was inclined, due to the asymmetry of the experimental setup, as already mentioned in [18]. Moreover, a good reproducibility of the crack mechanisms was observed at the macroscopic scale in comparison with the laminography tests performed on 1 mm thick specimens [18]. No crack initiation (small crack stable advance at the surface) was observed. A slight whitened zone can be noticed at the tip of the propagated crack in fig. 2c. This whitening is a sign of voiding through the thickness as already reported in many works [19, 14].

2.2.2. Features at (in-depth) microscopic scale

Images at the microscopic scale are displayed in fig. 3. The observations on a 2 mm thick CT-like specimen confirmed features that have already been described in [18]. Fig. 3a shows a vertical cut at mid-thickness plane, showing the reference image of the non deformed microstructure. Ring and horizontal stripe artefacts are present in all reconstructed images. At $\delta = 0.5$ mm, some microcracks emanating from the notch root are visible at mid-thickness in fig. 3b. Note that at the surface (fig. 2b), there was no observation that could be attributed to damage.

As reported by [1], fracture initiation can be a complex progressive process. The following SR-CL images highlighted these complex mechanisms of crack initiation and propagation. A horizontal cut (top view) in fig. 3c indicates that the maximum damage, represented by the cluster of penny shaped voids surrounded by yellow dashed line was located in the mid-thickness plane at a small distance (about 50 μm) from the initial notch root. Once initiated, this “microcrack” propagated radially in 4 directions through the crack plane: ahead, backward, transverse left and transverse right. These mechanisms of crack growth have already been reported for polyvinylidene fuoride and polyamide 6 respectively tested under steady strain rate (monotonic tensile) [12, 13] but also for medium density polyethylene tested under creep loading [8].

The crack front progression in these directions differed in their speeds. The expansion of the crack allows the introduction of 3 characteristic events that will extensively be used in the following sections:

- Step 1: Crack initiation (mid-thickness-small distance from the tip);
- Step 2: Backward crack front reaches the notch tip;
- Step 3: One of transverse crack front reaches the lateral surface, this is the first visible event at the macroscopic scale. Note that one crack initiation criterion is based on this third step: for instance J_{02} is based on a small propagation of 200 μm measured at the lateral surface.

In the case of the POM under study, the small crack advance at the lateral surface could not be observed since an instantaneous crack growth occured as soon as the backward crack reached the notch root (step 2).

As mentioned earlier, a constitutive model taking the porosity into account was used to simulate the load *versus* opening displacement of notched round bars with two different notch root radii [18]. The same model was used here for the small CT specimen in a finite element (FE) analysis, so as to estimate the load level at each step enabling also the load *versus* opening displacement (δ) to be plotted.

3. *J*-integral calculation assisted by finite element analysis

3.1. FE analysis

An in-house finite element (FE) code [4] was utilized throghout this study. The aforementioned constitutive model was extensively detailed in [18], where to account for the asymmetry of the boundary conditions in the SRL test, half of the CT-like specimen was meshed. In this paper, to alleviate the computation cost, only a quarter of the 2 mm thick specimen were modelled. A perfect symmetry was hence assumed. Fig. 4a depicts the mesh of this geometry whereas a zoom on the zone around the notch root is displayed in fig. 4b. The apparent front plane corresponds to the mid-thickness in the specimen. The outer surface is hidden (at the front of the back) in the views shown in fig. 4. The total mesh consists of 15,320 quadratic brick elements with a total of 52,899 degrees of freedom. The characteristic size of the mesh in fig. 4b is 50 μm. The uncracked section (remaining ligament) is blocked in the vertical direction. The plane at mid-thickness is blocked to lateral displacement.

Due to expected large deformation near the crack tip, an updated Lagrangian finite strain formulation was used. Moreover, the present constitutive model takes the strain-rate effects into account by utilizing a viscoplastic deformation component. Concerning the material coefficients calibration, an original inverse method procedure was used, combining global variables (stress, strain at the macroscopic scale) as well as local distributions of the porosity [18]. The material coefficients corresponding to the porosity were adjusted for a 1 mm thick CT-like specimen. For the sake of simplicity to account for the experimental stepwise loading procedure, the simulation has been run with a controlled opening displacement rate of 3 mm/min. Furthermore, a critical porosity of 0.7 was used allowing the elements reaching this porosity to be removed to simulate the crack growth. Recall that the initial porosity was assumed to be 0.01. The excellent agreement between experimental measures and simulated values supported the use of the same constitutive model with corresponding material parameters to model the specimens. Under these conditions, the load *versus* opening displacement ($F - \delta$) curves were produced by FE simulations. The use of erosion of elements to develop the critical porosity allowed the three steps of the load versus displacement described in section 2.2.2 to be simulated.

3.2. J-integral determination

It was not attempted here to use the numerical values of the load parameter J-integral based on FE method. Indeed, the validity of J-integral value with a finite strain formulation has not really been proven. In order to obtain J-integral close to "experimental" value, the numerical load *versus* opening displacement obtained by FE simulation was utilized. The evaluation of J-integral was based on the area under the $F - \delta$ curve [7, 2].

$$J = \eta \frac{U}{B(W - a_0)} \tag{1}$$

where, for CT specimen:

- B, W, a_0 are the thickness, the width and the initial crack depth respectively;
- $\eta = 2 + 0.522(1 - a_0/W)$;
- U is the area under the $F - \delta$ curve.

Here, the total area U was numerically integrated as follows:

$$U_T = \sum_{2}^{n_{max}} \frac{F_n + F_{n-1}}{2}(\delta_n - \delta_{n-1}) \tag{2}$$

where, F_n is the load at line n, δ_n is the corresponding opening displacement and n_{max} is the number total of experimental points in the $F - \delta$ curve, corresponding to a given step mentioned in section 2.2.2.

3.3. FE results

The results of the FE simulations and the corresponding J calculations are given in this section. Each figure deals with one of the three steps described in section 2.2.2. The evolution of “global” variables is depicted in a diagram where the load F and the J-integral value are plotted with respect to the applied δ. The local analysis is illustrated by a contour map of the porosity near the notch root where the elements for which the porosity has reached the critical value were removed. For the sake of simplicity, the contour map was drawn on undeformed meshes. Large strains induced highly deformed elements in the remaining ligaments as already shown by [18]. A numerical fracture surface could then be analyzed from these contour maps and it was possible to establish the link between each step to the corresponding point on the $(F - \delta)$ curve. In particular, the extent of the fracture surface where the load started to decrease could be identified. Fig. 5 shows an overview of the results.

Recall that step 1 corresponds to the appearance of the crack at mid-thickness and at a small distance from the initial notch root. This event was related to the time when the numerical simulation showed the first broken element at the same location. Fig. 5a left shows this first removed element representative to the features observed in fig. 3c. In the right diagram, it can be observed that the load was still increasing even if the experimental point was within the non linear part of the $(F - \delta)$ curve. The presence of the crack at mid-thickness is not yet detected at the macroscopic scale, on the $(F - \delta)$ curve. The evolution of J-integral is also shown in the diagram. The J-integral value at this characteristic event is rather high, due presumably to the reduced thickness of the specimen, yielding plane stress conditions.

Step 2 corresponds to the moment when the back crack front reached the initial notch root. Actually, from step 1 to step 2 a bridging matter is present between the notch root and the crack. This situation has already been reported for polyamide 6 tested under steady strain rate (monotonic tensile) [14, 5] but also for medium density polyethylene tested under creep loading [8]. The second step here is defined as corresponding to the moment when this bridge of matter has failed. Numerically, it is assigned to the moment when the first element touching the notch root surface is removed. Fig. 5b shows this situation and the corresponding diagram. The load has reached its maximum value here.

At step 3, the first element was removed at both lateral surface –due to symmetry– (fig. 5c left). The brittle crack was assumed to propagate rapidly at this stage. From step 2 to step 3, the load slightly decreased whereas the J-integral still increased. In fact, the extent of the crack growth is now significant so as to decrease the load. J-integral is still increasing because of a significant increase of the opening displacement compensating the load decrease. At the macroscopic scale step 2 to 3 can be considered as a propagation stage. The crack depth should be updated to obtain a more realistic J-integral value. This is out of the scope of this paper.

Table 1 displays the values of the load (noted as F_{st}) and the corresponding J-integral (noted as J_{st}) for each of the three steps. The subscript "st" deals here with that the parameters' value was related to the characteristic step as mentioned in section 2.2.2. It should be noted that the fracture toughness J_{Ic} has to be determined from J_{st} provided that a *criterion* is given. In the present work, attention is paid to two criteria based on macroscopic variables (($F - \delta$) curve or crack appearing at the surface):

- the maximum load F_C for which J_{st} critical value at F_C will be called J_{cr}^{Fc};
- the total crack growth at 0.2 mm, including crack tip blunting [7]. J_{st} value at step 3 where the crack front appearing at the *surface* will be assumed to have a total length of 0.2 mm. This critical value noted as J_{cr}^{Sf} follows the approach utilized to determine J_{02}. However, J_{cr}^{Sf} is not expected to fulfil all the requirements to be validated as the fracture toughness J_{02}.

Only the trends of these values will be discussed when the initial porosity of a layer of elements around the crack tip changes from that of the bulk material (f_0=0.01).

4. Discussion

4.1. Tooling/cutting conditions on polymers

This work consists of a contribution to study the influence of the sharp crack introduction technique into the fracture mechanics specimens on the fracture toughness J_{Ic} value of the same material. The techniques used to introduce sharp cracks consist of cutting or machining the polymer. They seem to induce a state consisting of a layer of matter near the notch root different from the bulk (remainder) of the specimen. Focusing on the cutting process of polymers, it may induce two different states at the crack tip depending on the tool geometry and inclination. Indeed, it was reported that the cutting may lead to that the tool touch the crack tip or not [16, 3, 20]. The two cases are noted as crack tip touching or non touching conditions. In the present paper the crack tip touching conditions are supposed to impose a compressive stress in a layer around the crack tip. As a consequence, if an initial porosity exists, this operation would close the voids, resulting in a local void volume fraction less than elsewhere in the specimen. Conversely, a crack tip non touching condition is similar to that of splitting a cantilever specimen with a wedge. Therefore, subsequent damage would appear in a layer of matter around the notch root. This is assumed here to be a layer in which the initial porosity is greater than that which is observed elsewhere in the specimen.

Benefiting from the FE results in the previous section, the aim is here to study numerically the effects of changing the initial porosity of a layer of elements in the vicinity of the notch root. This is assumed to be due to the introduction technique of the notch. To this end, a lower initial porosity is supposed to mimic a crack tip touching tool [20], leading therefore to stiffer crack tip layer elements and a less compliant specimen. Conversely a higher initial porosity in the layer is related to a crack tip non touching tool [20]. The crack tip layer of matter is likely to be softened leading to a more compliant specimen on the load *versus* displacement curve. The two cases will be discussed in terms of the induced variations on two critical J-integral values: J_{cr}^{Fc} and J_{cr}^{Sf}.

4.2. Finite element simulations

It was mentioned above that, in agreement with the stress distribution, the crack initiation appeared at a distance of about 100 μm from the notch root, that is to say four elements ahead (mesh size $\simeq$ 50μm). In order to keep this location of the crack initiation in the FE simulation, the layer was defined as being constituted of 4 elements surrounding the notch root. The set of elements corresponding to this layer is coloured in red in fig. 4b. Moreover, two different values of initial porosity within this layer, noted as f_0^L have to be defined. Recall that the initial porosity of the bulk was f_0=0.01, it was then decided to arbitrarily assign the values of $0.5f_0$ and $5f_0$ to f_0^L to ensure that they would not perturb the mechanisms of crack propagation – and hence the stress distribution ahead of the crack tip – in the three steps as presented in the previous sections.

Figs. 6-8 reveal the results of this numerical investigation. Figs. 6, 7 and 8 corresponding respectively to step 1, step 2 and step 3 as described in section 2.2.2. In each figure, the results given in section 3.2 have again be placed in the centre, label b). The upper figures show the case of the crack tip touching tool: f_0^L=0.005. Conversely, the figures labelled c) (bottom part) deal with crack tip non touching tool, leading to a more damaged layer: f_0^L=0.05. In each step and each value of f_0^L, both contour map of the porosity and $(F-\delta)$, $(J-\delta)$ curves are shown. Table 1 summarizes the characteristic values at each step.

<u>Step 1 (fig. 6)</u>

FE contour maps show that the location of crack initiation was respected. However, the exact location and the number of removed elements differ depending on f_0^L. Indeed, the number of removed elements decreases when f_0^L increases. The distance from the crack tip is the same for $f_0^L = f_0$ and $f_0^L = 0.5f_0$, whereas for $f_0^L = 5f_0^L$ the first broken element is situated at the interface between the layer and the bulk. $(F-\delta)$ and $(J-\delta)$ curves exhibit the same shapes. The crack initiation occurs in all cases in the non-linear part of the curve $(F-\delta)$. The lower f_0^L, the higher F_{st} and J_{st}. The results of the simulation capture the fact that the damage state of the crack tip layer can induce more or less compliant specimen response at the macroscopic scale. At this step, none of the two criteria could be selected. Indeed, the load is still increasing and the crack front did not reach the surface.

<u>Step 2 (fig. 7)</u>

This step corresponds to when the first element on the notch root is broken. The crack has already been propagating in the four directions as mentioned previously. The apparent fracture surface area decreases when f_0^L increases, with a particular observation for $f_0^L = 5f_0$ that is to say for the more damaged crack tip layer. Indeed, two cracks have developed, the first one grew laterally within the softened crack tip layer and the second crack has initiated in the bulk at the same location as both $f_0^L = 0.5f_0$ and f_0. It is to be noted that at this step the maximum load F_C was reached for $f_0^L = 0.5f_0$ and f_0 (fig. 7a-b). Therefore, the corresponding J_{cr}^{Fc} values were deduced for both cases (Table 1). A particular attention is paid here for the bulk material ($f_0^L = f_0 = 0.01$) for which the critical value of J-integral at maximum load is equal to 35 kJ/m^2. This value, noted as $J_{cr}^{Fc}(1\%)$ will be taken as reference to study the influence of the f_0^L.

Step 3 (fig. 8)

Actually, for $0.5f_0$ and f_0 cases the brittle crack was supposed to have been already propagated here. Nevertheless, the FE simulations were pursued to highlight the decrease in the load. The remaining case to be discussed consists of specimens with the more damaged crack tip layer ($f_0^L = 5f_0$). The contour map observation shows that the crack which has propagated laterally within the crack tip layer, reached first the lateral surface. Therefore, the crack initiation visible at the surface in this case is very close to the initial notch root. Whereas the load decreased for $f_0^L = 0.5f_0$ and f_0 (fig. 8a-b), the maximum load is obtained here for $f_0^L = 5f_0$ in fig. 8c. For this particular case, J_{cr}^{Fc} is selected at this step. Furthermore, this stage is assimilated to a crack propagation of 0.2 mm at the surface so that J_{cr}^{Sf} values were selected here. It is worth noting that:

- for $f_0^L = 5f_0$ in fig. 8c both criteria coincide at this step: $J_{cr}^{Fc} = J_{cr}^{Sf}$;
- for the bulk material ($f_0^L = f_0 = 0.01$), the critical value of J-integral assimilated to J_{02} is obtained here: $J_{cr}^{Sf}(1\%) \simeq 45$ kJ/m^2. For this second

criterion, this reference value will be utilized to study the influence of the f_0^L.

4.3. Effects of the tooling on J_{cr} values

The results obtained in the previous section were extended to $f_0^L = 0.1f_0$ and $f_0^L = 10f_0$. Depending on the criterion used (F_C or $\Delta a \simeq 0.2$ mm), the study of the influence of the initial porosity ahead of the notch root –considered here as due to the tooling– is carried out in this subsection.

4.3.1. Criterion on maximum load F_C (fig. 9)

Fig. 9a shows step by step the ratio between J_{st} and the reference value J_{cr}^{Fc} parameterized by f_0^L. Recall that F_C was reached at step 2 for $f_0^L \leq f_0$ (crack tip touching tool). The three upper curves in fig. 9a correspond to this case, where $J_{st}/J_{cr}^{Fc} = 1$ at step 2. In the same way, for $f_0^L > f_0$ (crack tip non touching tool), F_C is reached at step 3 where $J_{st}/J_{cr}^{Fc} = 1$. This case is represented by the two bottom curves in fig. 9a. It can be observed that:

- A criterion based on step 1 is not practical since there is no "signature" visible at the macroscopic scale. The J-integral values at this step is lower than J_{cr}^{Fc} of 25 % and 30 % for respectively lower and higher initial porosity attributed to crack tip touching and crack tip non touching tool;

- The maximum load criterion is consistent with crack tip touching tool inducing low initial porosity. In contrast, for higher initial porosity ahead of the crack tip (crack tip non touching technique), J-integral at step 2 differs for about -25 % in comparison with J_{cr}^{Fc};

- J-integral values at step 3 are higher of about 20 % than J_{cr}^{Fc} for crack tip touching techniques (lower initial porosity).

In fig. 9b, $J_{cr}^{Fc}(1\%) \simeq 35$ kJ/m^2 of the bulk material is considered as the critical value *without any influence of the tooling technique*. By plotting the evolution of the ratio $J_{cr}^{Fc}/J_{cr}^{Fc}(1\%)$, it can be observed that a decade of initial porosity set by the tooling technique ahead of the notch root increases the apparent critical value of J-integral. The maximum difference is higher in the case of crack tip touching tool (+23 %) than in the case of crack tip non touching technique (+10 %).

4.3.2. Criterion on Δa at surface (fig. 10)

The same analysis than in subsection 4.3.1 is carried out here, but using the criterion of the crack front appearing at the surface. For all case studies, step 3 is the critical step to be considered as reference. Recall that for crack tip touching technique ($f_0^L > f_0$), the maximum load is also reached at step 3: both criteria coincide here. It can be observed in fig. 10a that J_{step1} is lower of about -30 % than J_{cr}^{Fs}. In the same way J_{step2} is lower than J_{cr}^{Fs} but the difference depends on the f_0^L, ranging from -25 % to -10 % for $f_0^L = 10f_0$ and $f_0^L = 0.1f_0$ respectively.

The influence of the notch machining technique on J_{cr}^{Sf} based on $J_{cr}^{Sf} \simeq 45$ kJ/m^2, value for the bulk material can be summarized as follows:

- Crack tip touching tool process inducing lower initial porosity ahead of the notch root tends to increase the critical J-integral value. The maximum difference of 6 % is obtained for $f_0^L = 0.1f_0$;
- Conversely, crack tip non touching tool method leading to higher initial porosity ahead of the notch root tends to decrease more significantly the critical J-integral value. The maximum difference of -22 % is obtained for $f_0^L = 10f_0$.

4.4. Further discussion

The results obtained here raise some questions which merit discussion. In spite of a good trend shown by the FE simulations, the maximum difference in the critical J_{cr} values was about 20 %. For the polymer under study, some concepts have to be kept in mind:

- the approach utilized here is deterministic and assumes that the material is homogeneous. No account for the heterogeneity of the material microstructure and properties was considered. The scatter in these material properties might enlarge the effects obtained here on J_{Ic} value;

- The present analysis needs further quantification of the initial porosity ahead of the crack tip after the sharpening process, that is before running the fracture tests. Statistics on these data are the first input to study the abovementioned heterogeneity;
- it is known that the porous-plastic model used here is sensitive to both the initial value of the porosity and the mesh size. Work is currently ongoing to analyze this sensitivity.

Finally, the concept of softening/stiffening of the crack tip layer effects may be extended to study the influences of the material processing on the failure characteristics or even on the mechanical properties. For instance, the skin/core effects, the residual stress effects . . .

5. Conclusion

The present paper has shown experimental investigations at two scales. In addition to the currently measured variables at the macroscopic scale, SR-CL allowed through thickness observations in 3D of the microstructure during the deformation on CT-like specimen. The penny shaped crack initiated in the plane situated at mid-thickness, at a small distance from the initial notch root has been simulated. This crack expanded radially which led to the introduction of two further characteristic events: the step when the front of the back crack reached the notch root surface and the moment when the lateral crack front came out to the surface.

Benefiting from the damage based model elaborated in a previous study, these micro-mechanisms of crack initiation and growth were successfully simulated. From the numerical load *versus* opening displacement curve, the J-integral value could be determined, allowing therefore an evaluation of two critical values of the J-integral depending on the criterion used: J_{cr}^{Fc} and J_{cr}^{Sf} for maximum load and $\Delta a \simeq 0.2$ mm at the lateral surface, respectively.

The approach was then utilized to analyze the effects of variable initial porosity of the matter ahead of the notch root, assumed to be due to the sharp notch introducing technique on these critical J_{cr}. It has been shown that a crack tip touching tool, simulated by a stiffened layer of matter near the crack tip led to a less compliant specimen and a higher value of J_{cr}. Conversely, a non touching condition in cutting process, induced a damaged layer around the crack tip and thus a decrease in J_{cr}. Further work is needed to validate the results by measuring the initial porosity and the thickness of the layer of matter affected by the tooling process around the notch root. In addition, computations on thicker specimens to satisfy the plane strain requirement have to be performed.

[1] Agnelli, S., Baldi, F., Blackman, B., Castellani, L., Frontini, P., Laiarinandrasana, L., Pegoretti, A., Rink, M., Salazar, A., and Visser, H. (2015). Application of the load separation criterion in j-testing of ductile polymers: A round-robin testing exercise. *Polymer Testing*, 44:72–81.

[2] ASTM-D6068 (2010). *Standard Test Method for Determining J-R Curves of Plastic Materials*. ASTM International.

[3] Atkins, T. (2009). *The science and engineering of cutting*. Butterworth-Heinemann, 1st ed. Oxford.

[4] Besson, J. and Foerch, R. (1997). Large scale object-oriented finite element code design. *Comp. Methods Appl. Mech. Eng.*, 142:165–187.

[5] Cayzac, H., Saï, K., and Laiarinandrasana, L. (2013). Damage based constitutive relationships in semi-crystalline polymer by using multi-mechanisms model. *International Journal of Plasticity*, 51:47–64.

[6] Cheng, Y., Altapova, V., Helfen, L., Xu, F., dos Santos Rolo, T., Vagovič, P., Fiederle, M., and Baumbach, T. (2013). Multi-contrast computed laminography at anka light source. *J. Phys.: Conf. Ser.*, 463(1):012038.

[7] Hale, G. and Ramsteiner (2001). J-fracture toughness of polymers at slow speed. *Mechanics Testing Methods for Polymers Adhesives and Composites, D.R. Moore, A. Pavan, J.G. Williams (Eds.), ESIS Publication 28. Elsevier, Oxford (UK).*

[8] Hamouda, H. B. H., Laiarinandrasana, L., and Piques, R. (2009). A local approach to creep fracture by slow crack growth in an mdpe: Damage modelling. *Int. J. Pressure Vessels and Piping*, 86:228 – 238.

[9] Helfen, L., Baumbach, T., Mikulík, P., Kiel, D., Pernot, P., Cloetens, P., and Baruchel, J. (2005). High-resolution three-dimensional imaging of flat objects by synchrotron-radiation computed laminography. *Appl. Phys. Lett.*, 86:071915.

[10] Helfen, L., Morgeneyer, T., Xu, F., Mavrogordato, M., Sinclair, I., Schillinger, B., and Baumbach, T. (2012). Synchrotron and neutron laminography for three-dimensional imaging of devices and flat material specimens. *Int. J. Mat. Res.*, pages 170 – 173.

[11] Helfen, L., Myagotin, A., Mikulík, P., Pernot, P., Voropaev, A., Elyyan, M., Di Michiel, M., Baruchel, J., and Baumbach, T. (2011). On the implementation of computed laminography using synchrotron radiation. *Rev. Sci. Instrum.*, 82:063702.

[12] Laiarinandrasana, L., M., L., and Hochstetter, G. (2008). Fracture mechanics concepts applied to pvdf polymeric material exhibiting porosity, time and temperature dependency. *Proceedings of 17th European Conference on Fracture, September 2-5th, Brno, Czech Republic.*

[13] Laiarinandrasana, L., Morgeneyer, T., Proudhon, H., and Helfen, L. (2015). Cavitation in semi-crystalline polymers shown by x-ray tomography: application to constitutive modelling and durability. *Proceedings of 16th International Conference on Deformation, Yield and Fracture of Polymers, March 29 - April 2, Rolduc Abbey, Kerkrade, the Netherlands*, pages 35–38.

[14] Laiarinandrasana, L., Morgeneyer, T., Proudhon, H., N'Yguyen, F., and Maire, E. (2012). Effect of multiaxial stress state on morphology and spatial distribution of voids in deformed semicrystalline polymer assessed by x-ray tomography. *Macromolecules*, 45:4658–4668.

[15] Morgeneyer, T., Helfen, L., Sinclair, I., Proudhon, H., Xu, F., and Baumbach, T. (2011). Ductile crack initiation and propagation assessed via in situ synchrotron radiation computed laminography. *Scripta Mat.*, 65:1010 – 1013.

[16] Patel, Y., Blackman, B., and Williams, J. (2009). Determining fracture toughness from cutting tests on polymers. *Engineering Fracture Mechanics*, 76:2711 – 2730.

[17] Ricard, J. (2013). *Local approach to fracture on a semi-crystalline thermoplastic: the polyoxymethylene. Application: thermo-mechanical modelling of a screwing-threading process (in French).* PhD thesis, Ecole des Mines de Paris.

[18] Ricard, J., Guigné, F., and Laiarinandrasana, L. (2014). Damage and fracture mechanisms of polyoxymethylene: Multiscale experimental study and finite element modeling. *Engineering Fracture Mechanics*, 115:270–283.

[19] Schirrer, R., Fond, C., and Lobbrecht, A. (1996). Volume change and light scattering during mechanical damage in polymethylmethacrylate toughened with core-shell rubber particules. *J. Mater. Sci.*, 31:6409–6422.

[20] Williams, J., Patel, Y., and Blackman, B. (2010). A fracture mechanics analysis of cutting and machining. *Engineering Fracture Mechanics*, 77:293 – 308.

Table and figures

Table 1: Loads F_{st} and corresponding J_{st} values calculated for the three steps, for various initial porosities f_0^L of the layer of elements ahead of the notch root. For the bulk material, $f_0 = 0.01$

f_0^L	Load and J-integral	Step 1	Step 2	Step 3
0.001	F_{st} (N)	279	281	278
	J_{st} (kJ/m^2)	32.95	43.07	47.72
0.005	F_{st} (N)	274	278	275
	J_{st} (kJ/m^2)	31.38	37.57	45.91
0.01	F_{st} (N)	271	275	274
	J_{st} (kJ/m^2)	30.49	35.06	44.86
0.05	F_{st} (N)	261	265	271
	J_{st} (kJ/m^2)	26.96	29.16	38.9
0.1	F_{st} (N)	254	259	268
	J_{st} (kJ/m^2)	24.44	26.44	35.05

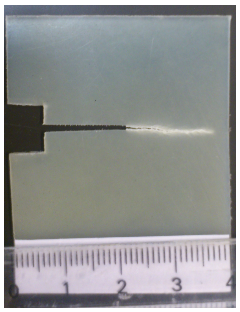

a)

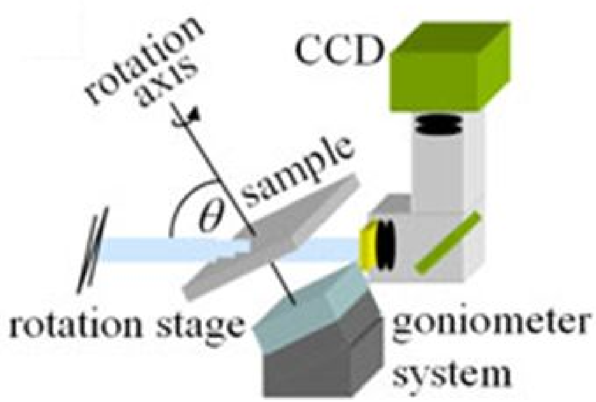

b)

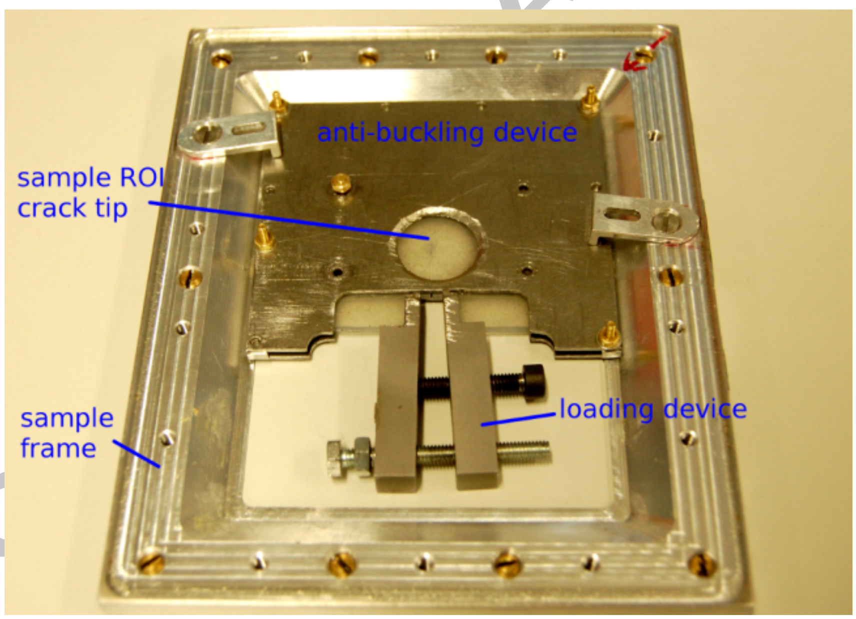

c)

Figure 1: a) POM CT-like specimen b) Principle of SR-CL; c) Apparatus mounted to the SR-CL platform to load the CT-like specimen.

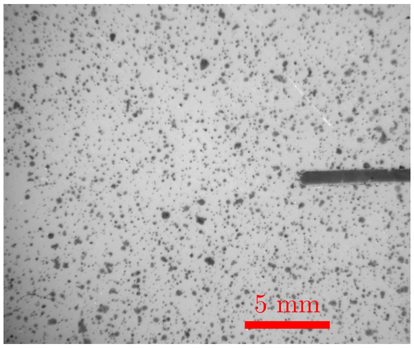

a) Initial state

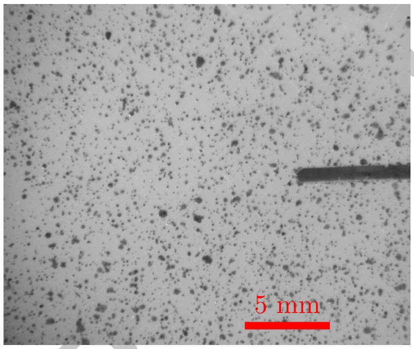

b) Deformed at $\delta = 0.5$ mm

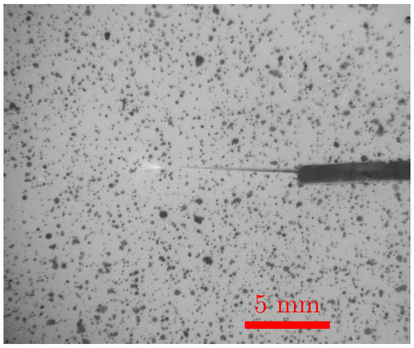

c) Rupture at $\delta \leq 1$ mm

Figure 2: Pictures of the lateral surface of the CT specimen in the vicinity of the notch root; a) non deformed notch root; b) $\delta = 0.5$ mm, opened notch root, no visible whitening at the surface; c) $\delta = 1$ mm, after brittle failure, whitened zone around the tip of the propagated crack

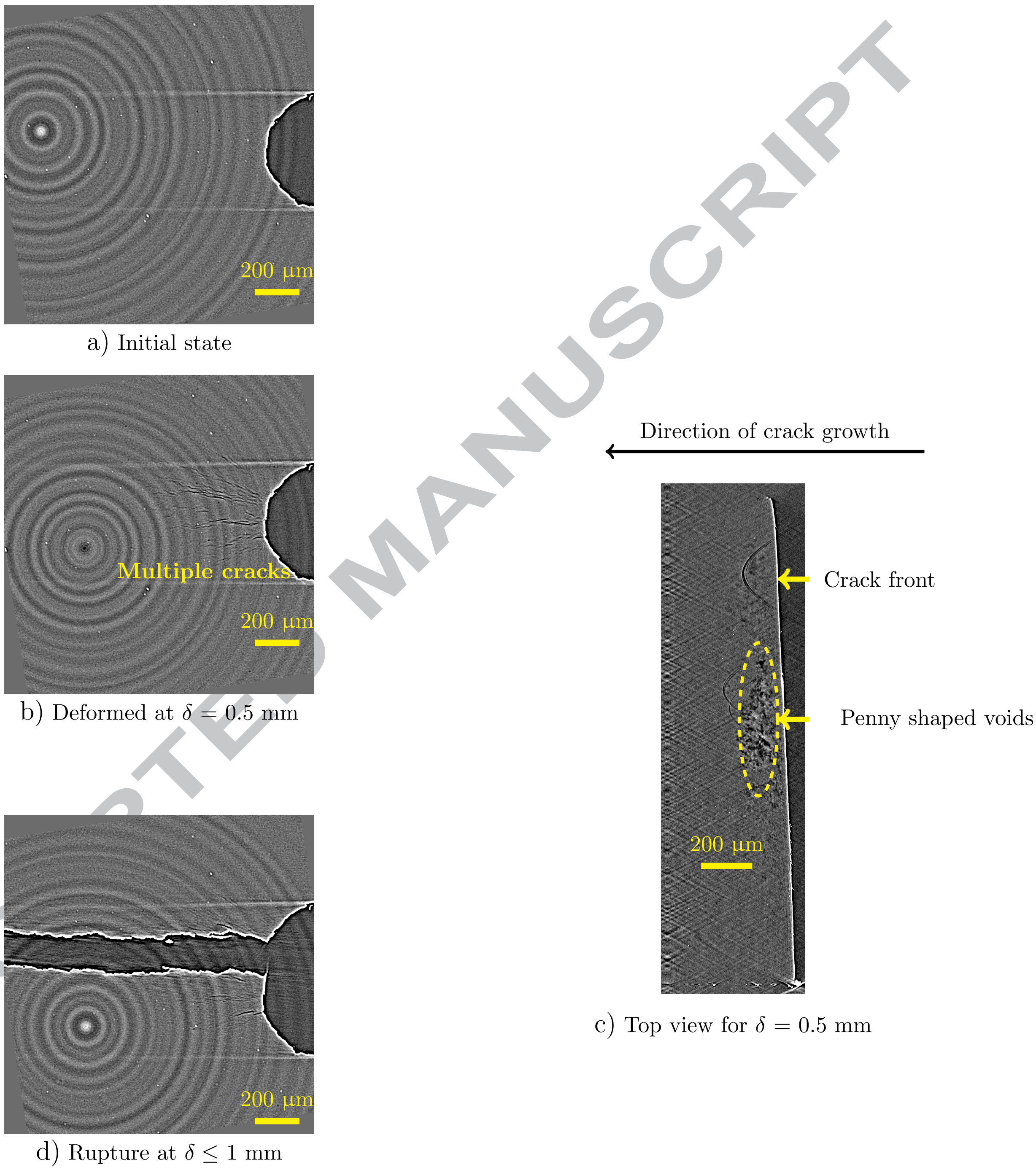

Figure 3: Observations at the microscopic scale: a) initial state; b-c) δ=0.5 mm, maximum voids at mid-thickness and at a small distance from the notch root; d) after brittle failure

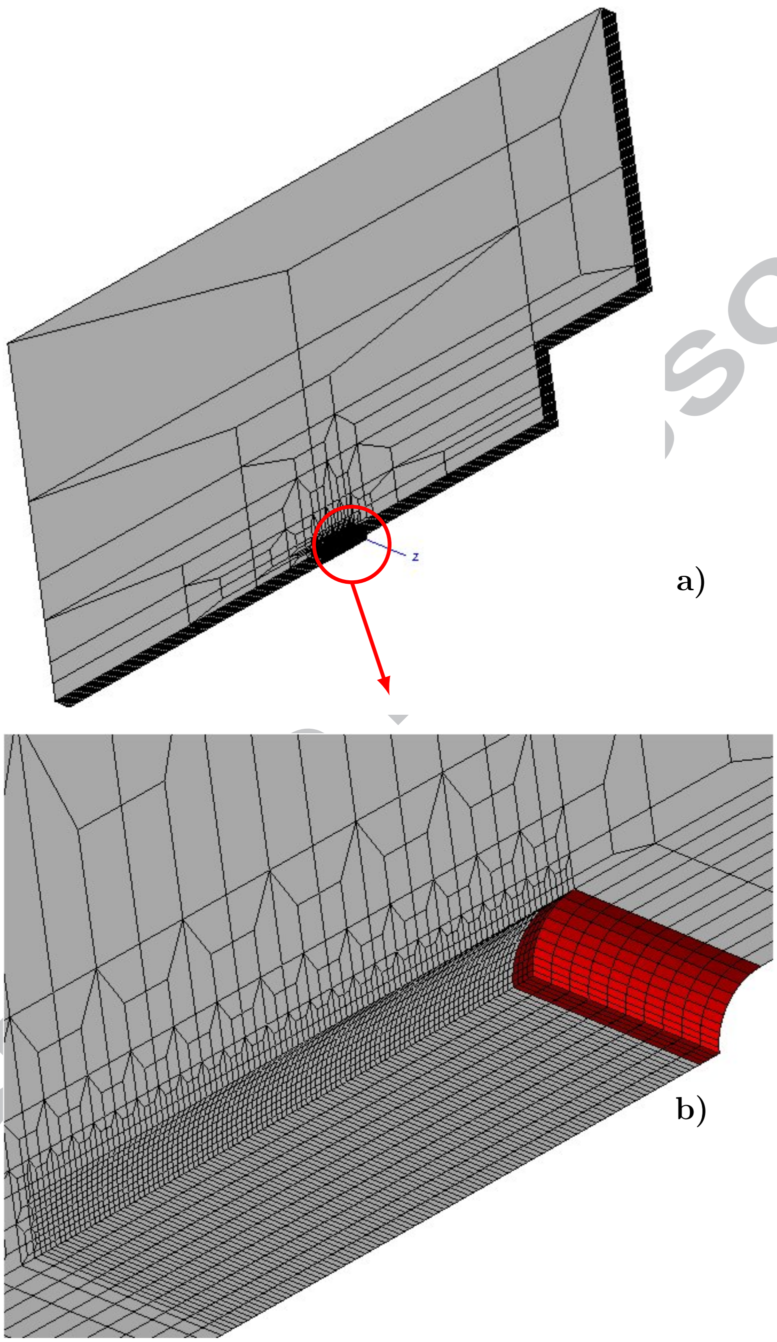

Figure 4: Meshing of CT specimen tested *in-situ* by laminography; a) quarter of the specimen; b) Details of refined meshes near the notch root. In red, layer of elements in the vicinity of the notch root (initial porosity f_0^L).

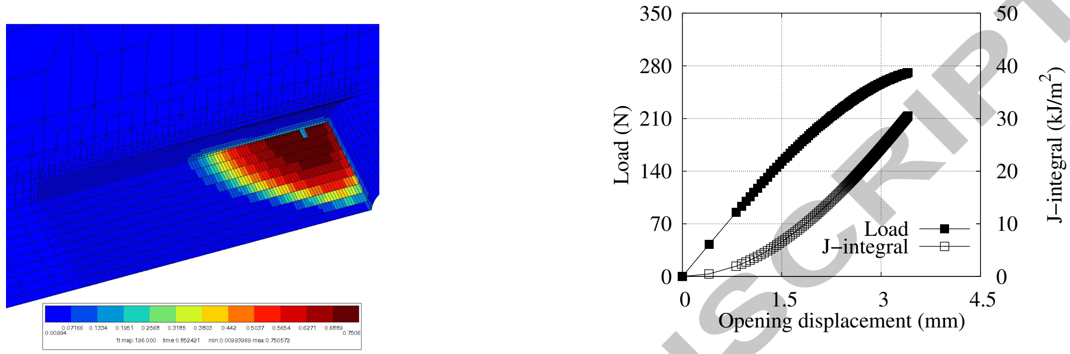

a) **Step 1**

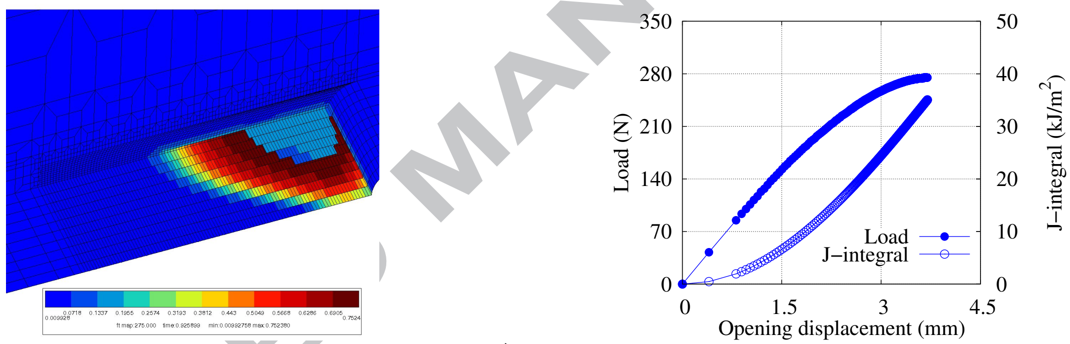

b) **Step 2**

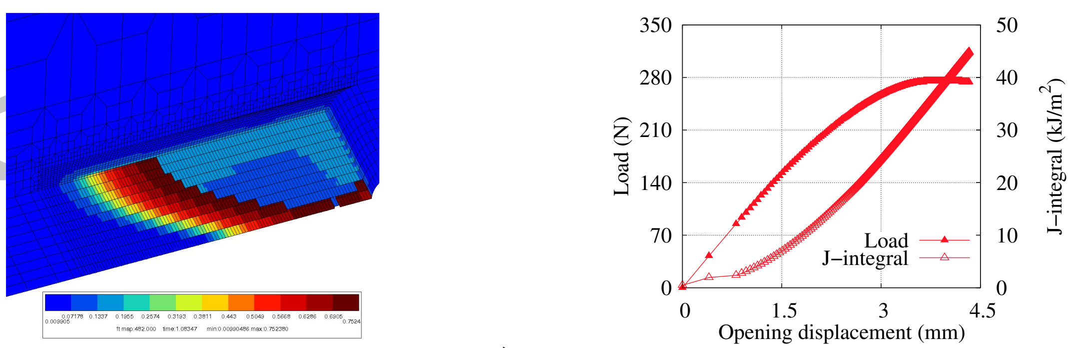

c) **Step 3**

Figure 5: Contour map of the porosity and the $(F - \delta)$ curve at each charcateristic event: a) Step 1: at crack initiation; b) Step 2: when the back crack front reaches the notch root; c) Step 3: when the lateral crack front reaches the surface.

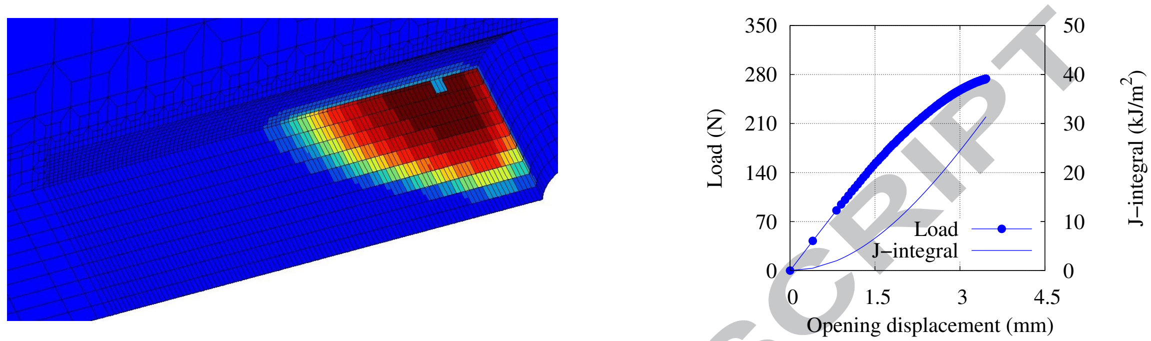

a) $f_0^L = 0.5 f_0$ **= 0.005**

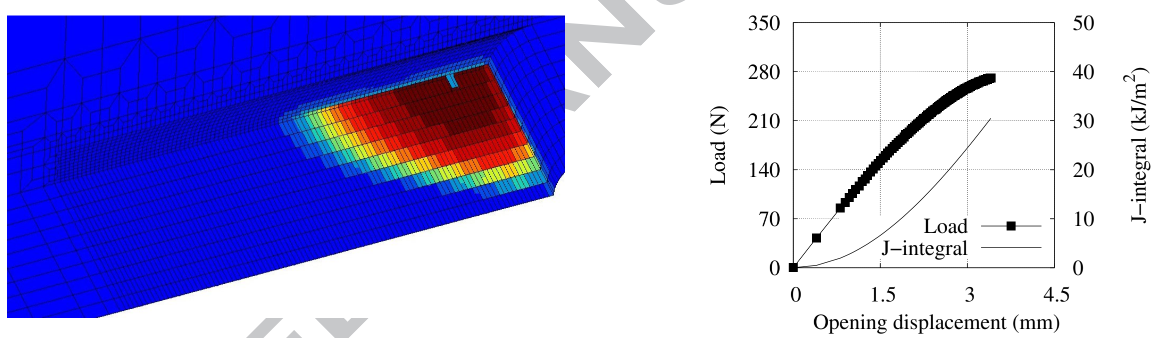

b) $f_0^L = f_0$ **= 0.01**

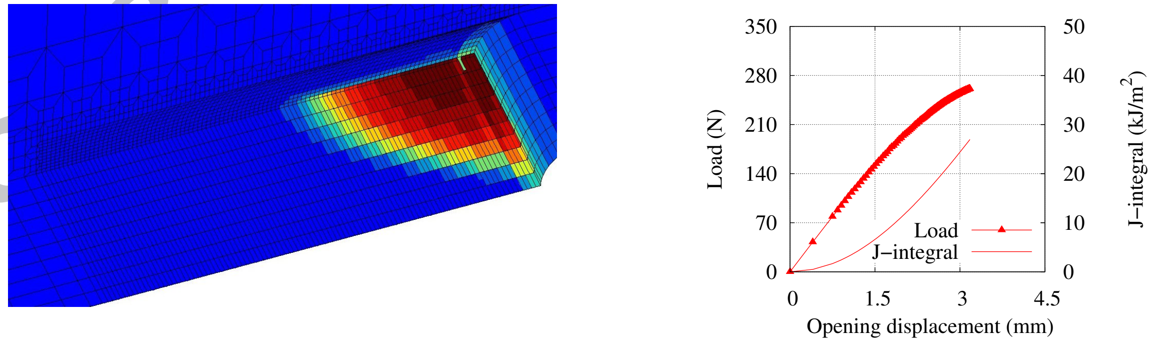

c) $f_0^L = 5 f_0$ **= 0.05**

Figure 6: Contour map of the porosity and the $(F - \delta)$ curve for step 1, for various initial porosity on a layer of elements around the crack tip

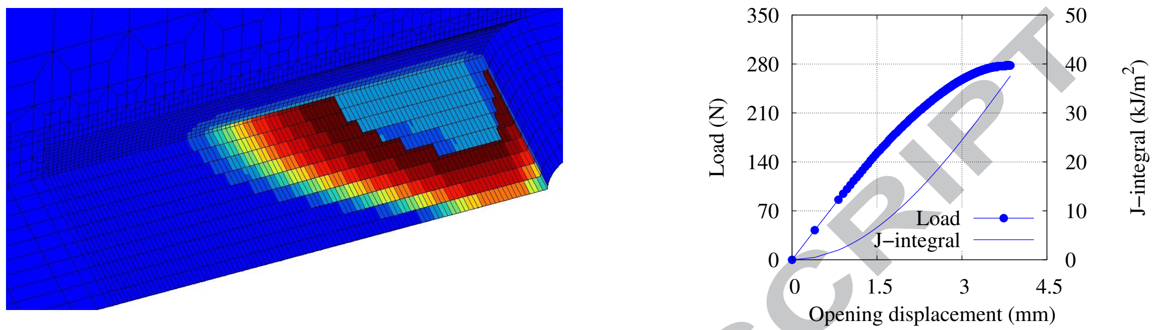

a) $f_0^L = 0.5 f_0 = \mathbf{0.005}$

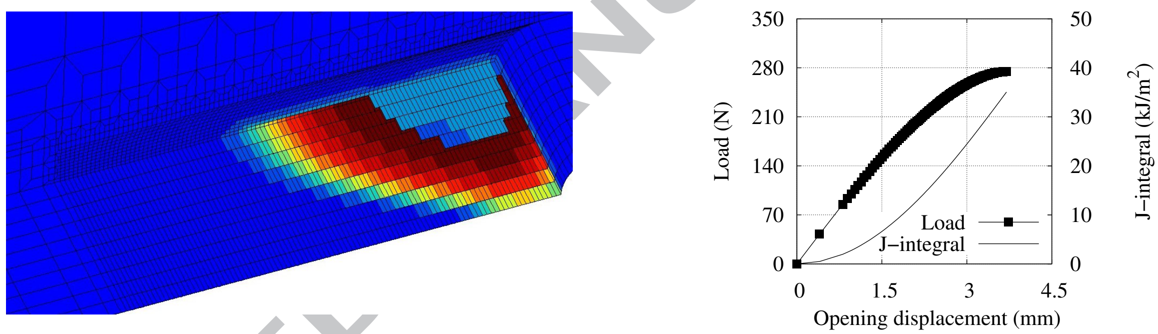

b) $f_0^L = f_0 = \mathbf{0.01}$

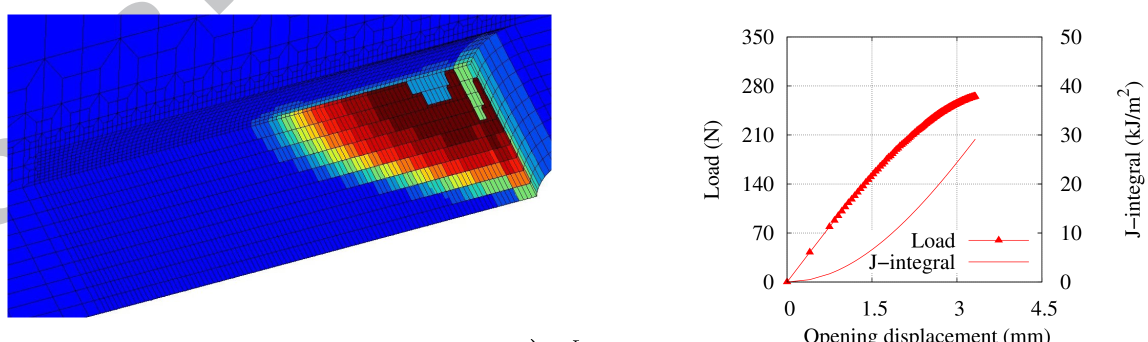

c) $f_0^L = 5 f_0 = \mathbf{0.05}$

Figure 7: Contour map of the porosity and the $(F - \delta)$ curve for step 2, for various initial porosity on a layer of elements around the crack tip

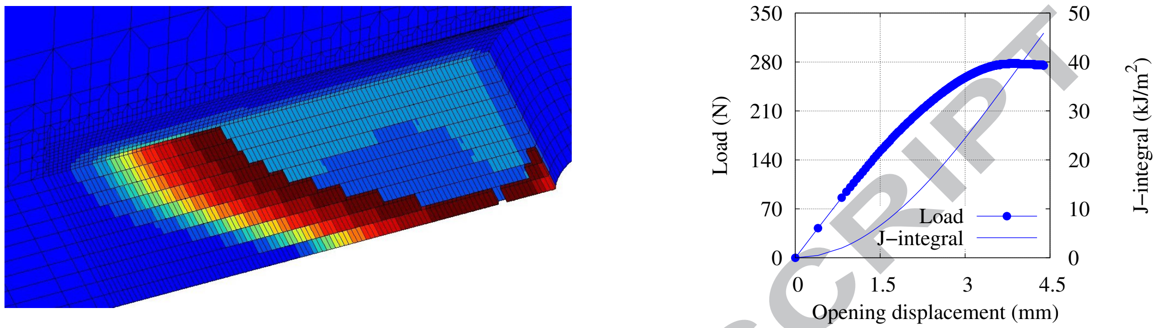

a) $f_0^L = 0.5 f_0 = \mathbf{0.005}$

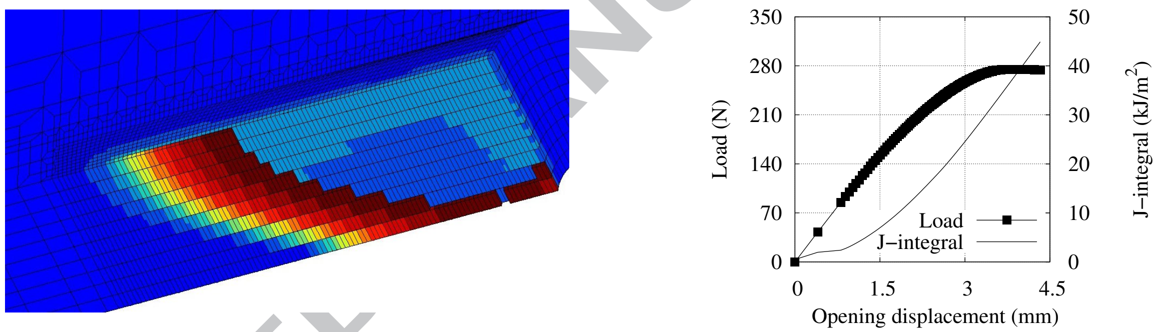

b) $f_0^L = f_0 = \mathbf{0.01}$

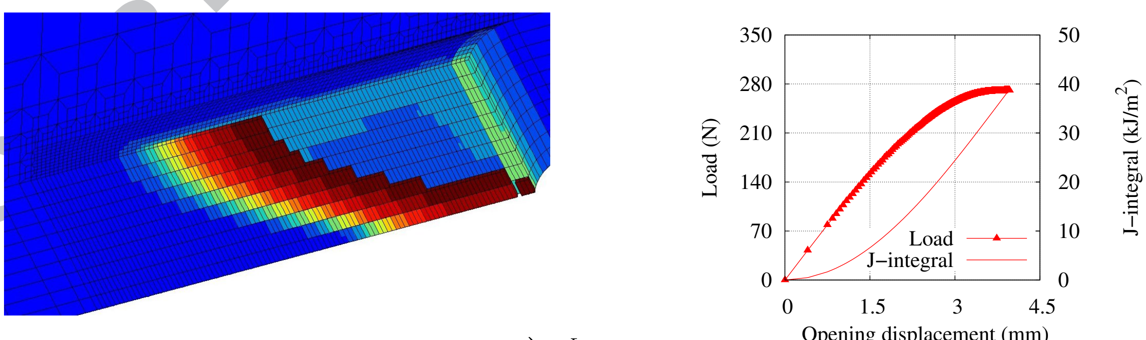

c) $f_0^L = 5 f_0 = \mathbf{0.05}$

Figure 8: Contour map of the porosity and the $(F - \delta)$ curve for step 3, for various initial porosity on a layer of elements around the crack tip

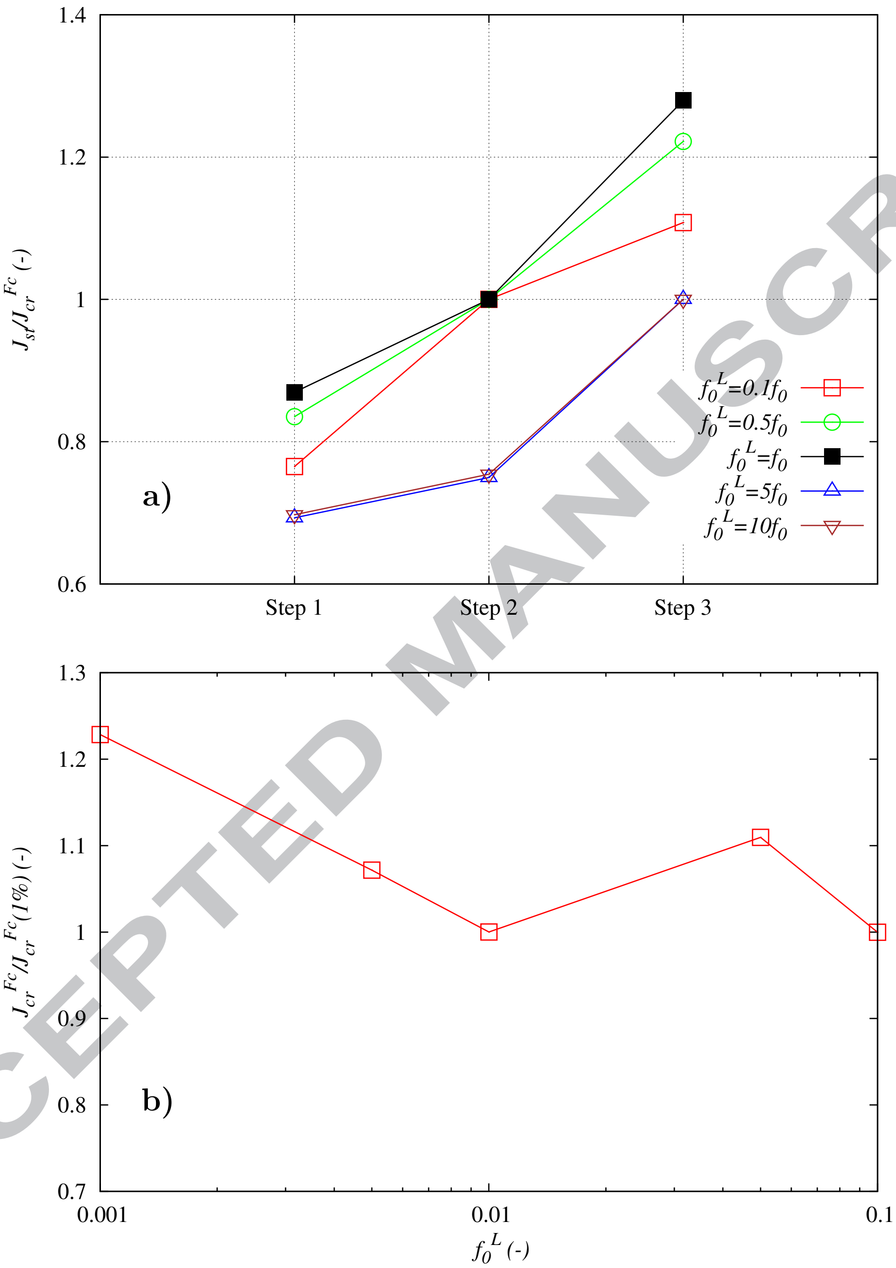

Figure 9: Evolution of the characteristic J-integral values by using the maximum load criterion: a) J_{st} with respect to the step of the crack growth mechanisms and parameterized by the initial porosity of a layer of elements ahead of the notch root (f_0^L); b) influence of f_0^L on the critical J_{cr}^{Fc}.

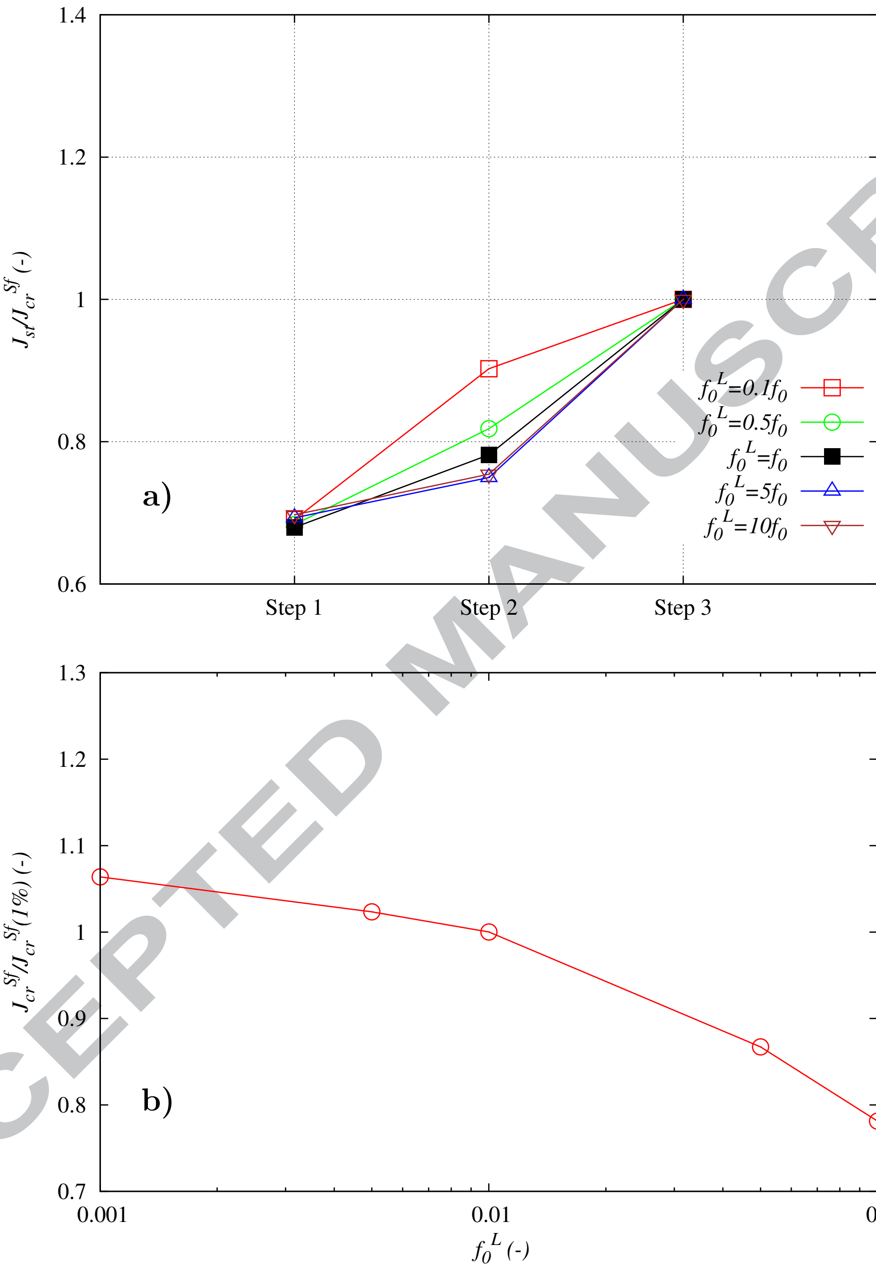

Figure 10: Evolution of the characteristic J-integral values by using Δa at the lateral surface as criterion: a) J_{st} with respect to the step of the crack growth mechanisms and parameterized by the initial porosity of a layer of elements ahead of the notch root (f_0^L); b) influence of f_0^L on the critical J_{cr}^{Sf}.

Nomenclature

a_0 : initial crack length

B : specimen thickness

CT : Compact Tension specimens abbreviation

DMTA : Dynamic Mechanical Thermal Analysis

DSC : Differential Scanning Calorimetry

♎ : opening displacement

J : J-integral

J_{st} : J-integral value at a given step

J_{cr}, J_{cr}^{Fc}, J_{cr}^{Sf}: Critical J-integral value, based on maximum load F_C and on a small crack at the surface S_f

F : load

F_C : load at crack initiation

f_0 : initial porosity of the POM

f_0^L : initial porosity assigned to the layer of element around the crack tip

POM : polyoxymethylene

❒ : notch root radius

SR-CL : Synchrotron Radiation Computed Laminography

U : area under the (F-♎) curve = total energy required to extend the crack

W : specimen width

Highlights

Local approach to fracture to investigate notch introduction process in polymers

X-ray laminography to inspect in 3D the damage mechanisms

Characterization of crack growth mechanisms on CT specimen

FE simulations with dedicated damage-based model capturing the micro-mechanisms

Effects of the notch introducing technique on the fracture toughness